Vignesh Ahilan, Camila Cabral de Barros, Gourav Dhar Bhowmick, Makarand M. Ghangrekar, M. Mangir Murshed, MichaelaWilhelm, Kurosch Rezwan

Microbial fuel cell performance of graphitic carbon functionalized porous polysiloxane based ceramic membranes

Journal Article as: peer-reviewed accepted version (Postprint)

DOI of this document*(secondary publication): 10.26092/elib/2494

Publication date of this document: 22/09/2023

* for better findability or for reliable citation

Recommended Citation (primary publication/Version of Record) incl. DOI:

Vignesh Ahilan, Camila Cabral de Barros, Gourav Dhar Bhowmick, Makarand M. Ghangrekar, M. Mangir Murshed, Michaela Wilhelm, Kurosch Rezwan,
Microbial fuel cell performance of graphitic carbon functionalized porous polysiloxane based ceramic membranes,
Bioelectrochemistry, Volume 129, 2019, Pages 259-269, ISSN 1567-5394,
https://doi.org/10.1016/j.bioelechem.2019.06.002.

Microbial fuel cell performance of graphitic carbon functionalized porous polysiloxane based ceramic membranes

Vignesh Ahilan [a], Camila Cabral de Barros [a,c], Gourav Dhar Bhowmick [b], Makarand M. Ghangrekar [d], M. Mangir Murshed [e,f], Michaela Wilhelm [a,*], Kurosch Rezwan [a,f]

[a] University of Bremen, Advanced Ceramics, Am Biologischen Garten 2, IW3, 28359 Bremen, Germany
[b] Department of Agricultural and Food Engineering, Indian Institute of Technology, Kharagpur, 721302, India
[c] Department of Materials Engineering, Federal University of Santa Catarina (UFSC), 88040-900 Florianopolis, SC, Brazil
[d] Department of Civil Engineering, Indian Institute of Technology, Kharagpur, 721302, India
[e] University of Bremen, Institute of Inorganic Chemistry and Crystallography, Leobener Straße 7, D-28359 Bremen, Germany
[f] MAPEX Center for Materials and Processes, University of Bremen, 28359 Bremen, Germany

ARTICLE INFO

Article history:
Received 21 March 2019
Received in revised form 4 June 2019
Accepted 4 June 2019
Available online 8 June 2019

Keywords:
Polymer derived ceramic
Proton conducting membrane
Microbial fuel cell
Graphene oxide
Multiwall carbon nanotube

ABSTRACT

Proton-conducting porous ceramic membranes were synthesized *via* a polymer-derived ceramic route and probed in a microbial fuel cell (MFC). Their chemical compositions were altered by adding carbon allotropes including graphene oxide (GO) and multiwall carbon nanotubes into a polysiloxane matrix as filler materials. Physical characteristics of the synthesized membranes such as porosity, hydrophilicity, mechanical stability, ion exchange capacity, and oxygen mass transfer coefficient were determined to investigate the best membrane material for further testing in MFCs. The ion exchange capacity of the membrane increased drastically after adding 0.5 wt% of GO at an increment of 9 fold with respect to that of the non-modified ceramic membrane, while the oxygen mass transfer coefficient of the membrane decreased by 52.6%. The MFC operated with this membrane exhibited a maximum power density of 7.23 W m^{-3} with a coulombic efficiency of 28.8%, which was significantly higher than the value obtained using polymeric Nafion membrane. Hence, out of all membranes tested in this study the GO-modified polysiloxane based ceramic membranes are found to have a potential to replace Nafion membranes in pilot scale MFCs.

1. Introduction

Microbial fuel cells (MFCs) are a promising alternative bioelectrochemical technology, that converts the chemical energy presents in the organic matter of wastewater directly into electrical energy through the metabolic oxidation of exoelectrogenic bacterial species. The organic materials present in the anodic chamber of the MFC are oxidized to produce electrons, which are further transported from the anode to the cathode through an external circuit. Meanwhile, protons released out of the above oxidation process, travel from the anode to the cathode *via* a separable membrane, which separates anodic and cathodic chamber [1,2]. Since MFCs are capable of simultaneously performing wastewater treatment and electricity generation, it has attracted much attention from researchers in recent years [3]. One of the most expensive component of the MFC is its membrane. Polymeric Nafion membranes have been traditionally used as proton exchange membranes (PEM) not only for MFCs, but also for hydrogen fuel cells [4], owing to their high ionic conductivity and reasonable chemical stability in oxidative-reductive environments [5]. However, the practical applicability of MFCs on the industrial scale is limited due to high costs of Nafion membranes, biofouling that occurs during long-term operation and low mechanical strength that does not allow them to withstand higher hydrostatic pressures [6,7], that is likely to occur in full scale MFCs. In order to overcome the drawbacks of this technology and optimize the performance of MFC, a proper membrane material must be selected. Zhu et al. investigated membrane-less MFC and came up with their advantages such as no issues like membrane biofouling and additional internal resistance because of membrane [8]. However, membrane-less technology is not ideal for long term operation of MFC, because of its high oxygen and substrate crossover rate, which can severely deteriorate the performance of the MFC [9].

Multiple membrane-related research studies have been conducted to develop an inexpensive polymeric membrane material for MFCs such as polytetrafluoroethylene, sulfonated polystyrene— ethylene —butylene—polystyrene, polyethersulfone/sulfonated polyether ether ketone and sulfonated polyethersulfone [10–13]. However, the resulting polymeric membranes were not suitable for scaling up of the MFC due to their low mechanical stability. In the last few years, considerable progress has been made in the development of mechanically

* Corresponding author.
E-mail address: mwilhelm@uni-bremen.de (M. Wilhelm).

https://doi.org/10.1016/j.bioelechem.2019.06.002

stable ceramic membranes for application in MFCs, which exhibit many advantages over polymeric membranes. Pasternak et al. evaluated performance of MFCs utilizing four different ceramic materials and found that the MFCs containing pyrophyllite and clayware ceramic membranes produced the highest power densities of 6.93 and 6.86 W m^{-3}, respectively [14]. To further increase the power density of MFC, composite clay based ceramic membranes with cation exchange fillers such as montmorillonite and kaolinite were proposed [15]. Ghadge et al. reported that the addition of 20% montmorillonite to a clay based ceramic membrane increased the power density of MFC to 7.55 W m^{-3}, which was higher than that of the polymeric Nafion membrane [15].

Among other membrane materials, polymer derived ceramics (PDC), mainly composed of silicon oxycarbide (SiOC)-based materials, are of significant interest because of their unique properties including high mechanical stability, large oxidation resistance and *micro*/*meso*/*macro* porous hierarchical structure [16–18]. These PDC characteristics can be tailored by selecting a proper synthesis method, varying the pyrolysis temperature and changing the material composition [19,20]. In particular for application in MFCs, porous PDC membranes have been synthesized with good physical properties, including high ion exchange capacity (IEC), high cation transport number and low oxygen permeability. Furthermore, the addition of cation exchange fillers such as montmorillonite and $H_3PMo_{12}O_{40}/SiO_2$ to the PDC matrix can significantly enhance its functional properties at low pyrolysis temperatures. However, both these fillers ultimately decomposed at a higher pyrolysis temperature (1000 °C), which negatively affected the membrane performance [21].

Currently, substantial attention is being paid to carbon allotropes such as graphene oxide (GO) and multiwall carbon nanotubes (MWCNTs) due to their high thermal and mechanical stabilities, large ionic conductivity and good oxygen barrier properties [22–25]. Incorporation of GO or MWCNTs into a polymer matrix improves various physical and chemical characteristics of the membrane, including its ion conductivity, mechanical strength and degree of oxygen permeation [24,26]. For instance, Khilari et al. reported that the addition of GO to a polyvinyl alcohol—silicotungstic acid composite polymer membrane significantly increased its ionic conductivity and decreased the oxygen diffusion rate, which enhanced the overall power generation and chemical oxygen demand (COD) removal efficiency of the MFC [26]. Similarly, Li et al. reported that the CNT-modified polymeric Nafion membrane exhibited a 1.5 fold increase in the mechanical strength and a five-fold increase in the proton conductivity [27].

In the present study, porous PDC composite membrane modified with GO and functionalized MWCNTs were prepared and evaluated for their potential as the separator material for application in MFC. First, a series of composite PDC membranes with different contents of GO and MWCNTs were synthesized through a facile pressing technique. The fabricated membranes were characterized in terms of their pore size distributions, surface characteristics, IECs, oxygen permeability and mechanical stability, which were compared with the parameters of the standard commercial polymeric Nafion membrane. Furthermore, the performance of MFCs using PDC and its composite membranes was evaluated in terms of the power density, internal resistance, COD removal efficiency and coulombic efficiency (CE).

2. Experimental methods

2.1. Chemicals required

A commercial hydrophobic oligomeric methyl-phenyl polysiloxane powder (H44 Silres® Wacker Chemie), Bis(trimethoxypropyl)silyl amine (BISA, ABCR Dr. Braunagel GmbH & Co. KG), ethanol (99%, Alpha Aesar) as the solvent, ammonia (25%, Alpha Aesar) and water for catalyzing the polymerization reaction were used to prepare the ceramic membranes with GO and MWCNT (Nanochem) as filler materials. The GO prepared using synthetic graphite powder (Timical Timrex® SFG75), sulfuric acid (conc. H_2SO_4, Sigma Aldrich), potassium permangenite ($KMnO_4$, Sigma Aldrich), hydrogen peroxide (30 wt% H_2O_2, Sigma Aldrich), hydrochloric acid (37% HCl, Sigma Aldrich). Functionalization of MWCNT was carried out using nitric acid (65% HNO_3, Sigma Aldrich) and sulfuric acid (conc. H_2SO_4, Sigma Aldrich).

2.2. Graphene oxide synthesis

The GO was produced from graphite powder using a modified Hummers method. Briefly, 3 g of graphite powder was added to 70 mL of concentrated H_2SO_4 and well agitated for several minutes followed by the addition of 9 g $KMnO_4$ using an ice bath. The solution was transferred to a flask containing 150 mL of deionized (DI) water and then placed in an oil bath at 40 °C under stirring. After vigorously stirring for 15 min, the oil temperature was increased to 95 °C, after which the reactants were stirred for another 15 min. Subsequently, 500 mL of DI water was added to the reaction mixture followed by the slow addition of 15 mL H_2O_2 (30%) and overnight stirring at room temperature. After that, the liquid was washed with concentrated HCl and DI water until its pH reached to 7.0 and then ultrasonically agitated for 30 min. At this point, the aqueous dispersion contained two different materials: GO and non-exfoliated graphite oxidized to graphite oxide, which were easily separated by centrifugation.

2.3. Pretreatment of multiwall carbon nanotube

Functionalization of MWCNT was performed using mixture of HNO_3 and H_2SO_4 acids in a molar ratio of 1:3 to create a solution with a final volume of 20 mL. Pristine MWCNTs (100 mg) were added to this solution and the mixture was treated by magnetic stirring vigorously for 3 h at room temperature. The functionalized MWCNTs were then purified by extraction from the residual acids by dilution with distilled water and centrifuged repeatedly until the pH of the solutions reached to approximately 6.0. After the purification process, the oxidized samples were dried at 80 °C for over-night.

2.4. Polymer derived ceramics membrane synthesis

In a typical synthesis, an equimolar ratio of H44 and BISA (1:1) was dissolved in the ethanol dispersion of a filler material inside the round bottom flask placed in an oil bath at 70 °C under stirring. Subsequently, 3.27 mL of ammonia and 3 mL of distilled water were slowly added to the reaction mixture. The reaction was performed under reflux until a stable polymeric solid material was obtained. After that, the solvent was removed by drying and cross-linking in air - first at 140 °C for 1 h and then at 200 °C for 2 h. The cross-linked PDC sample was ground to fine powder *via* high-energy ball milling and pressed to a monolithic structure. The produced membranes were pyrolyzed at 1100 °C for 4 h under nitrogen atmosphere. The schematic representation of the synthesis procedure is shown in Fig. 1.

2.5. Sample notation

Sample nomenclature was based on the notation PDC:xGO–zzz and PDC:yCNT-zzz, where PDC represents SiOC, GO with weight fraction x in the starting material, CNT with weight fraction y, and zzz is the pyrolysis temperature (Table 1).

3. Physicochemical membrane characterization

3.1. Material characterization

The X-ray diffraction (XRD) pattern of the samples was measured using SEIFERT XRD 3003 research edition, United States, with Cu-Kα radiation, 2θ from 10° to 90° in steps of 0.02° and a counting time per step

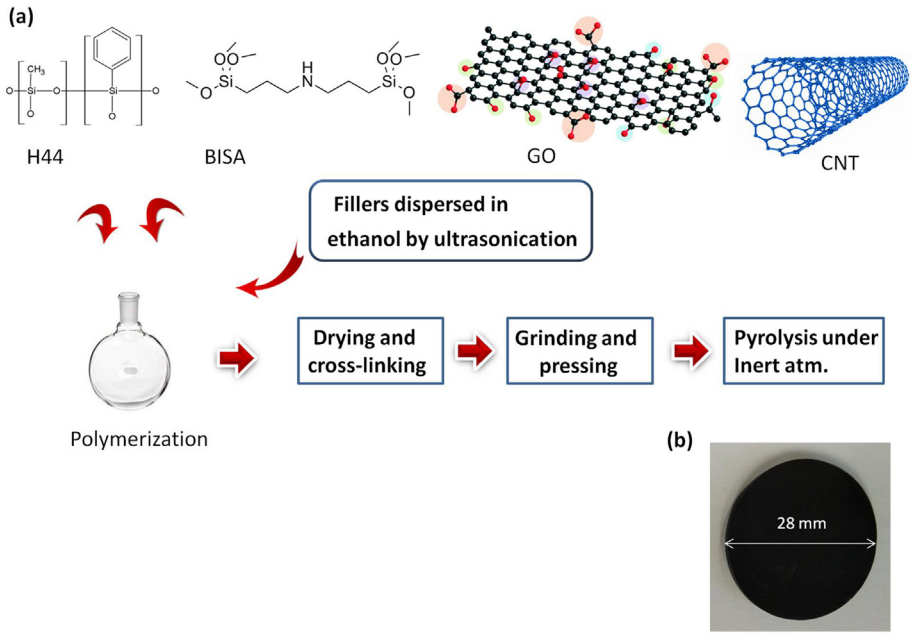

Fig. 1. (a) Synthesis flowchart of PDC composite membrane (b) Sample prepared at 1100 °C.

of 2° min^{-1}. Raman spectra were recorded at ambient condition on a LabRam ARAMIS (Horiba Jobin Yvon) Micro-Raman spectrometer equipped with a laser working at 785 nm and less than 20 mW. The usage of a 50× objective (Olympus) with a numerical aperture of 0.75 provides a focus spot of about 2 μm diameter when closing the confocal hole to 200 μm. The spectra were collected in the range from 800 cm^{-1} to 2000 cm^{-1} with a spectral resolution of approximately 1.2 cm^{-1} using a grating of 1800 grooves mm^{-1} and a thermoelectrically-cooled charge coupled device (CCD) detector (Synapse, 1024 × 256 pixels). Each spectrum was baseline corrected with the 'LabSpec' software (Horiba Jobin Yvon). The specific surface area was measured by recording nitrogen adsorption and desorption isotherms at 77 K (Belsorp-Mini, Bel Japan). The samples were heated at 120 °C for 3 h as a pretreatment in order to remove adsorbed water molecules from the material surface. Porosity and mean pore sizes of the samples were measured *via* mercury intrusion porosimetry (Pascal 140/440, Porotec). The vapor adsorption was measured by placing 0.5 g of dry powdered PDC composite materials in an open glass container in closed Erlenmeyer flasks filled with the solvent of water or heptane in equilibrium with its vapor phase at room temperature. The samples were weighed before and after a 24-h measurement period in order to determine the vapor adsorption of the materials. Later, the adsorption capacity of the solvent was recalculated using the Brunauer–Emmett–Teller (BET, Bell Japan Inc) to determine the specific surface area of the materials.

3.2. Mechanical stability

According to German Standard Code DIN 52292, ring-on-ring bending test was carried out to measure the bending strength of the ceramic membrane. The test samples, with a radius r_3 and a thickness S, were placed on a supporting ring while the force was applied with a load ring perpendicular to the sample surface. A Zwick/Roell material-testing machine type Z005 (Zwick/Roell GmbH, Ulm, Germany) equipped with a 5 kN load cell was used to measure the maximum force F at the moment of failure. The ratio r_1: r_2 between the radius of the load ring r_1 and the supporting ring r_2 was set to 1:5. The initial load was set to 0.5 N, the test velocity to 0.5 mm min^{-1} and the number of trial samples were three. For all samples, the Poisson's ratio of $\mu = 0.12$ was assumed. The bending strength σ in mega pascal (MPa) was estimated using Eq. (1).

$$\sigma = \frac{3(1+\mu)}{2\pi}\left[\ln\frac{r_2}{r_1} + \frac{(1-\mu)}{(1+\mu)}\cdot\frac{{r_2}^2-{r_1}^2}{2{r_3}^2}\right]\cdot\frac{F}{S^2} \quad (1)$$

Table 1
Prepared membrane compositions with equal mole ratio of H44 and BisA and pyrolysed at 1100 °C.

Membranes	Graphene oxide (wt%)	MWCNT (wt%)
PDC	–	–
PDC:0.5GO	0.5	–
PDC:2GO	2	–
PDC:0.5CNT	–	0.5
PDC:2CNT	–	2.0

3.3. Ion exchange capacity

The IEC of each membrane was determined using titration method [28]. The membrane was first equilibrated with 100 mL of 1 M HCl solution for 72 h. After that, it was removed from the acid solution and rinsed with DI water to remove the surface-adsorbed ions on the membranes. It was then transferred to 50 mL of 1 M NaCl to exchange the H^+ to Na^+ over equilibration for 24 h. Afterward, the membrane was removed and the NaCl solution was titrated with 0.005 M NaOH to determine the amount of H^+ present in the solution. The IEC was expressed in milliequivalents of H^+ per gram of dry membrane using Eq. (2).

$$IEC = (V_{NaOH} \times M_{NaOH})/W_{dry} \quad (2)$$

Where, V_{NaOH} is the volume of NaOH solution consumed, M_{NaOH} is the molarity of NaOH (0.005 M), and W_{dry} is the weight of dry sample.

3.4. Oxygen diffusion coefficient

The oxygen permeability of the membrane was measured as described in other studies [29]. The DI water-filled in one chamber was continuously purged with N_2 gas for 30 min and maintained in an anaerobic state with an oxygen concentration of less than 0.02 mg L^{-1}; whereas, the DI water-filled in another chamber was aerated continuously to maintain a near-saturation dissolved oxygen (DO) condition.

The oxygen concentration in the first chamber was monitored using a DO probe at regular time interval of 15 min and the oxygen mass transfer and diffusion coefficient were determined by using Eqs. (3) and (4), respectively.

$$k_o = -\frac{v}{At} \ln\frac{C_{oc} - C_{oa}}{C_{oc}} \quad (3)$$

$$D_o = K_o * L_{th} \quad (4)$$

Where, v is the volume of chamber in cm^3, A is the area of membrane in cm^2, t is time in s, C_{oc} is the oxygen concentration in the second chamber in mg L^{-1}, C_{oa} is the oxygen concentration in the first chamber in mg L^{-1}, L_{th} is the thickness of the membrane in cm.

3.5. Microbial fuel cell setup and operations

Four MFCs, with two chambered aqueous cathode configuration, were fabricated using 30 mm thick poly-(methyl-methacrylate) fibre sheet with a working volume of 70 mL each for anodic and cathodic chamber. The carbon felt (Panex_35 Zolex Corporation) was used as cathode and anode (with a surface area of 16 cm^2 each) separated by the synthesized membrane separators. These carbon felts were pretreated by consecutive washing with 1 N HNO_3, 30% ethanol and deionized water until the neutral pH was obtained. The felts were then dried in a hot air oven at 100 °C followed by thermal treatment in muffle furnace at 400 °C for 30 min and cooling in vacuum desiccators for further use. Electrodes were connected with concealed copper wires and the connections were coated with polymer glue to protect from corrosion. Operating voltage (OV) was measured over 100 Ω of external resistance. Resin and glue in fixed proportion were used to make the MFCs water resistant. Nafion 117 membrane was used as PEM for the control MFC in order to compare the performance of the synthesized membranes with it, after pre-treating with 3% H_2O_2 solution for one hour followed by dipping in DI water for two hours.

The inoculation in anodic chamber of MFCs was done using anaerobic mixed consortia with a volatile suspended solids (VSS) concentration of 19.90 g L^{-1} and total suspended solids (TSS) of 30.20 g L^{-1}, collected from a septic tank, IIT Kharagpur, after pre-treating it by applying heat (100°C for 15 min). The synthetic wastewater with sucrose as carbon source was fed to the MFCs with initial organic matter concentration of around 3 g of COD L^{-1} supplemented with trace elements [30]. All the MFCs were kept in an open environment under ambient temperature varying from 28 ± 2 °C. Each MFC was operated for 15 feed cycles to gain representative performance results. The MFCs were run in replica as well to check the precision of the results in batch mode with fresh feeding frequency of 3 days. The schematic of MFC used is shown in **Fig. S2**.

3.6. Analytical measurements

The OV and open circuit voltage (OCV) of the MFCs were measured on daily basis using a digital multi-meter with a data acquisition unit (Agilent Technologies, Malaysia). The polarization curve was graphed by altering the external resistance from 10,000 to 10 Ω using a resistance box (GEC05R Decade Resistance Box, Bangaluru, India). The power (P, in W) generated from the MFCs was determined as E^2_{cell}/R_{ext}, which upon dividing with anodic chamber volume gave maximum volumetric power density (mW m^{-3}). The internal resistance of MFC was measured from the slope of the polarization plot of voltage *vs.* current. The net amount of coulombs getting recovered from the theoretical coulombs present in the synthetic wastewater were expressed as CE according to Eq. (5).

$$CE = \frac{M_s \int I.dt}{F.b_{es}.V_{an}.\Delta COD} \quad (5)$$

Where, M_s is the molecular weight of the substrate in g mol^{-1}, F is the Faraday's constant = 96,485C $mole^{-1}$, I is the current in mA, t is the retention time in h, b_{es} is the generated electrons per mol of substrate oxidized, V_{an} is the anodic chamber liquid volume in L and ΔCOD is the change in substrate concentration over a batch cycle in g L^{-1}.

Normalized energy recovery (NER) was also calculated for all the MFCs on the basis of the volume of wastewater treated over the time (kWh m^{-3}) using Eq. (6).

$$NER = \text{Energy output/Treated wastewater volume} \quad (6)$$

The COD of untreated and treated wastewater samples and VSS of the anaerobic sludge were analyzed according to Standard Methods [31].

4. Results and discussion

4.1. Phase analysis

The XRD was used to investigate the phase evolution of PDC membrane pyrolyzed at 1100 °C (Fig. 2a). The observation of broad peaks from the XRD pattern in between 20 ° and 30 ° significantly show that SiOC is amorphous in nature. Such amorphous SiOC network can be generated by the substitution of two divalent oxygen ions by one tetravalent carbon atom within the SiO_2 network. The composition of a stoichiometric SiOC, consisting solely of Si—O, Si—C bonds and some excess free carbon, this clearly explained by Kleebe et al. [32]. Raman spectroscopy was analyzed to understand the graphitic nature of carbon present in the SiOC and in the filler materials (Fig. 2b). The Raman spectrum of graphitic carbon shows the usual three bands at around 1340, 1582 and 2717 cm^{-1}, which are designated as the D, G, and 2D bands, respectively. However, the Raman spectrum of these samples displayed only two major peaks at 1343 and 1585 cm^{-1} in the range from 800 to 2000 cm^{-1}, corresponding to the D band due to structural defects and the G band representing the degree of order of graphene structure, respectively [33]. In detail, the G-band is attributed to the first order scattering of the E2g phonon of the sp2 carbon-carbon bond; while the D-band represents the defect sites associated with vacancies and grain boundaries [34]. The carbon with sp2 hybridization such as graphene or graphite has lower I_D/I_G ratio, which indicates lower defect concentration. However, GO is not a purely sp2 system however a highly disordered one with a significant sp3 content. Hence, contrary to the standard sp2 materials, the increase of defects in GO would produce a decrease of the I_D/I_G ratio. This is because there would be more sp2 carbon atoms surrounding the defects [35].

The observed D and G band of PDC-1100 sample showed a ratio of 1.06, which significantly demonstrated the presence of free carbon in the SiOC matrix. The I_D/I_G intensity ratio increased from 0.96 for PDC:0.5GO-1100 to 1.02 for PDC:2GO-1100. It showed that a significant decrease in the defect domains upon reduction of the GO phase in the PDC:2GO-1100 sample [36]. This illustrated that GO presence in PDC:0.5GO-1100 is comparatively stable probably due to grafting of GO functional group with the SiOC matrix. A similar effect was observed by Lou et al. in an investigation on ceramic supported GO composite membrane [37]. Further addition of 2 wt% of GO resulted in segregation of GO along with the graphitic free carbon in the PDC Matrix, which resulted in partially reduced GO during pyrolysis at 1100 °C. On the other hand, I_D/I_G ratio of PDC:0.5CNT-1100 and PDC:2CNT-1100 material was 1.02 for both. This demonstrated graphitic carbon nature with increased band ratio of above 1, due to the segregation of MWCNT along with free

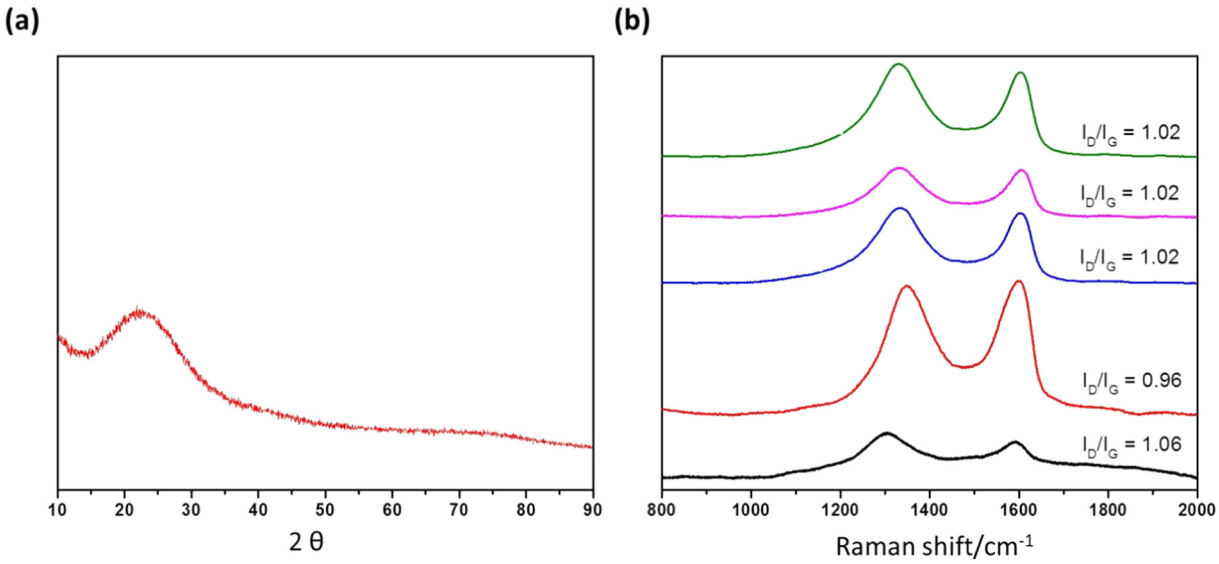

Fig. 2. (a) X-Ray diffraction pattern of PDC-1100 membrane; (b) Raman spectroscopy of PDC-1100 (black); PDC:0.5GO-1100 (red); PDC:2GO-1100 (blue); PDC:0.5CNT-1100 (pink) and PDC:2CNT-1100 (green).

carbon presence in the PDC matrix [33]. The Raman spectra of GO and MWCNT materials is shown in supporting information **Fig. S1**. The I_D/I_G of GO pyrolysed at 1100 °C increased, which clearly showed the transformation of GO to reduced GO.

4.2. Specific surface area and pore size distribution

Unlike the polymeric membranes, whose ion transfer properties depend on the presence of functional groups, porous ceramic membranes are not ion-selective and transport ions through their porous structures when the membrane surface is hydrophilic [38]. Therefore, studying the micro-, *meso* and macroporous structural properties of PDC membranes are very important for determining their suitability for application in MFCs. In this work, the micro-meso-porosity of the prepared samples were characterized by recording nitrogen adsorption-desorption isotherms (Fig. 3a). According to the IUPAC classification, the shapes of the isotherm curves obtained for the sample pyrolyzed at 1100 °C correspond to type III isotherms, indicating that the material has only a macroporous structure. The incorporation of GO and MWCNTs (with contents of 0.5 and 2 wt%, respectively) into the PDC matrix increased its specific surface area due to the presence of high surface area fillers [39]. The BET specific surface area (Fig. 3b) increased in the order of PDC-1100 < PDC:0.5CNT-1100 < PDC:0.5GO-1100 < PDC:2CNT-1100 < PDC:2GO-1100 from 4 up to 25 $m^2\ g^{-1}$.

Macroporous size distributions and open porosities of the membranes were determined by mercury intrusion porosimetry (the histograms are shown in Fig. 4a). The pore size distribution in the PDC membranes did not change significantly with addition of GO filler material. The average pore size of PDC-1100, PDC:0.5GO-1100 and PDC:2GO-1100 were 325 nm, 407 nm and 344 nm, respectively. On the other hand, the opposite trend was observed for PDC composite with MWCNT, since the average pore size of PDC:0.5CNT-1100 and PDC:2CNT-1100 membrane was 735 nm and 619 nm, respectively. This phenomenon might be caused by the partial decomposition of MWCNTs at 1100 °C leading to the evolution of carbon-containing gases and formation of large voids and defects in the membrane structure due to the dispersion of MWCNTs across the polysiloxane matrix during synthesis. MWCNTs can easily agglomerate, bundle, and entangle in a polymer matrix, which can produce defects such as large pores [40,41]. In addition, all PDC and composite membranes prepared

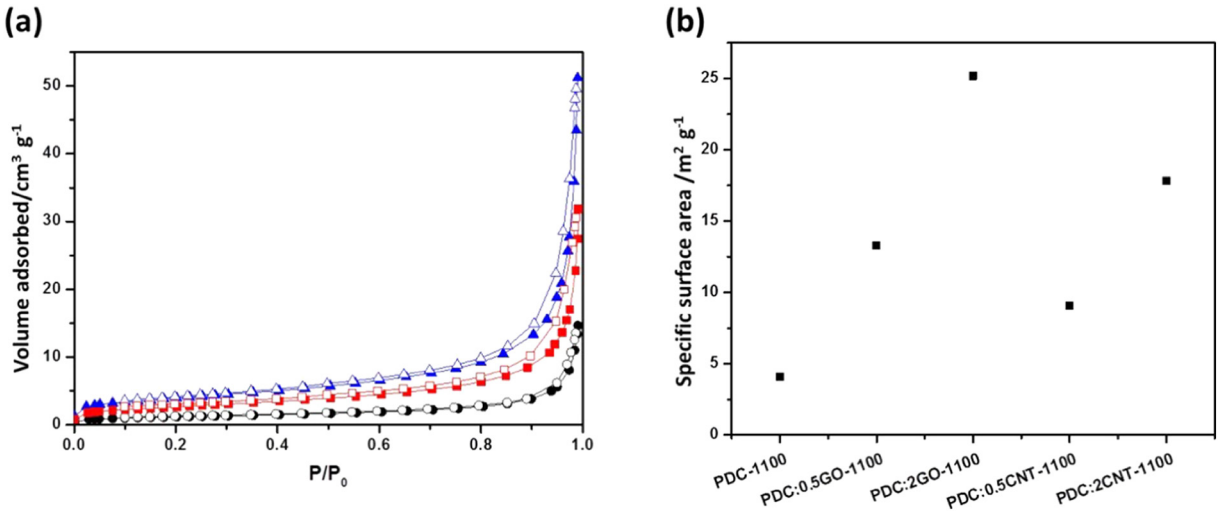

Fig. 3. (a) Nitrogen adsorption desorption isotherms of PDC-1100 (black); PDC:0.5GO-1100 (blue) and PDC:0.5CNT-1100 (red), (b) Specific surface areas of pyrolyzed membranes calculated (BET) from nitrogen adsorption isotherm.

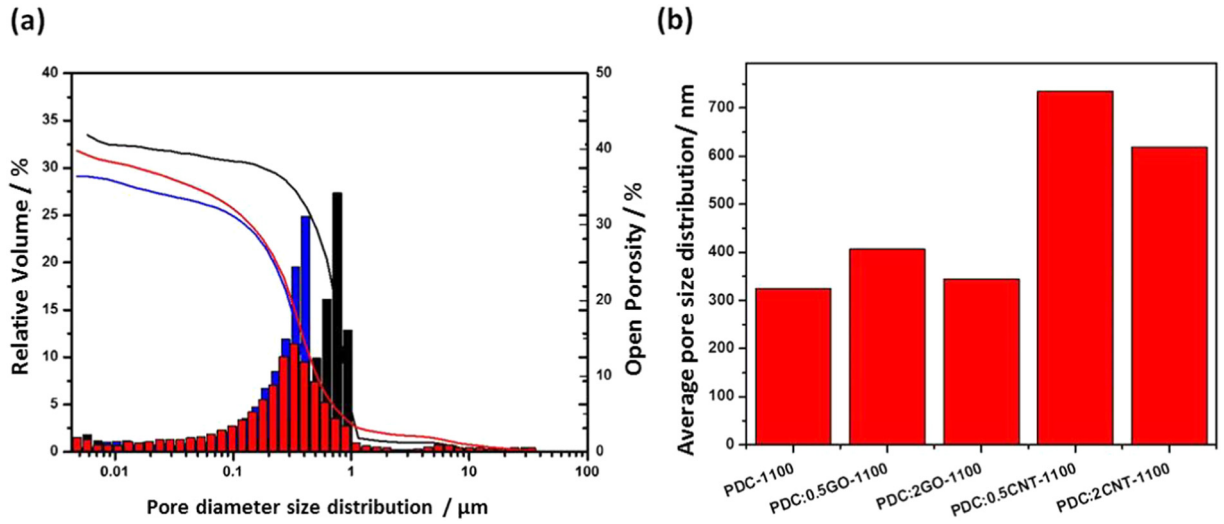

Fig. 4. (a) Pore size distribution *versus* relative pore volume and open porosity curves obtained from Hg-porosimetry histrogram of PDC-1100 (red); PDC:0.5GO-1100 (blue) and PDC:0.5CNT-1100 (black) (b) Average pore size of prepared PDC membranes.

in this study exhibited open porosities between 31 and 43%, which were suitable for application in MFCs and facilitated the diffusion of protons from one chamber to another by the osmotic and electro-osmotic drags [42].

4.3. Hydrophilic characteristics

The hydrophilic properties of the membrane promote the adsorption of water molecules in its porous structure that act as proton transfer carriers [43]. Since an accurate water contact angle is difficult to measure for a porous structure, the adsorption of polar and non-polar solvent vapors at the pore walls (such as water and n-heptane) was performed to examine the hydrophobic/hydrophilic behavior of the samples tested (Fig. 5). The amount of adsorbed vapors (in mmol m^{-2}) were related to the specific surface area measured by recording N_2 adsorption-desorption isotherms. In the samples pyrolyzed at 1100 °C, most of the hydrophobic methyl and phenyl groups of the preceramic polymers (H44 and BISA) were decomposed, which increased their degrees of hydrophilicity [44]. Although all the membrane samples were hydrophilic in terms of the water-to-heptane ratio

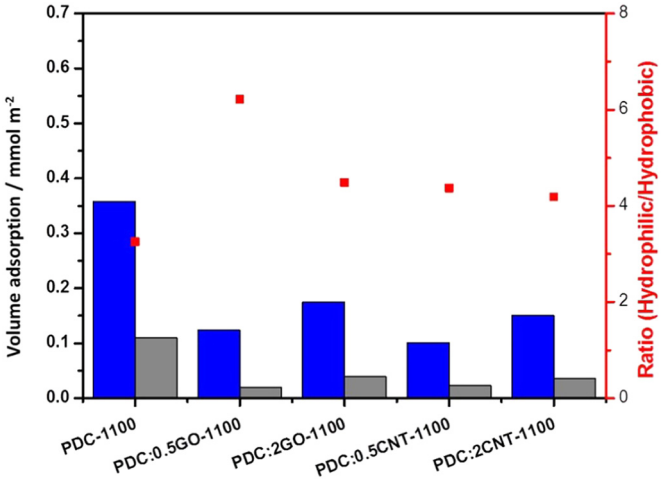

Fig. 5. Water (blue) and n-heptane (gray) vapor adsorption at 25 °C for as prepared membrane materials at 1100 °C; Red dot represents its adsorption ratio.

(greater than 1), the specimens without fillers were clearly less hydrophilic than other samples due to the presence of hydrophilic functional property of the filler materials. The phenomenon was observed for the PDC-1100 and PDC:0.5GO-1100 specimens, which demonstrated an increment of 91.1% after the addition of 0.5 wt% GO. Likewise, Ganesh et al. reported that the GO-modified polysulfone membrane exhibited hydrophilic properties because of the negatively charged surface of the GO filler [44]. This is mainly because of oxidized graphene sheets (or 'GO sheets') having their basal planes decorated mostly with epoxide and hydroxyl functional groups, in addition to carbonyl and carboxyl functional groups located presumably at the edges (Lerf–Klinowski model). These oxygen functionalities rendered the GO layers to be hydrophilic and water molecules can readily intercalate into the interlayer galleries. The GO can therefore be also thought of as a graphite-type intercalation compound with both covalently bound oxygen and non-covalently bound water between the carbon layers.

The strong bonding of GO functional group across the free carbon presence in the PDC matrix led to prevent the reduction of GO for 0.5 wt% GO loading [45]. However, further addition of 2 wt% GO into the PDC membrane resulted in a slight decrease in the water-to-heptane ratio, which is related to the existence of reduced GO in the SiOC matrix and this inhibited the adsorption of water molecules in its structure. Hence, due to the high loading of GO in the PDC matrix, it leads to segregation of GO filler material without bounding with free carbon presence in the PDC matrix. This segregated GO, thermally reduced to reduced GO during pyrolysis. The presence of reduced GO in the PDC:2GO-1100 membrane led to a less hydrophilic nature compared to PDC:0.5GO-1100 membrane. Stankovich et al. also reported that the transformation of GO to reduce GO tends to be hydrophobic in nature due to the absence of hydrophilic sites [45]. On the other hand, samples prepared with MWCNT (PDC:0.5CNT-1100 and PDC:2CNT-1100) exhibited water-to-heptane ratios of 4.36 and 4.18, which were 34% and 28% higher than the values obtained for bare PDC-1100, respectively. The surface characteristics of PDC:0.5CNT-1100 and PDC:2CNT-1100 is almost similar. This is because of the tendency of MWCNT didn't change gradually with increase in filler content, that evidently shown in Raman spectrum.

4.4. Ion exchange capacity

The IEC values of the PDC composite membranes were obtained by a back titration method (Fig. 6a). Their magnitudes determined for the PDC:0.5GO-1100 and PDC:2GO-1100 membranes were 9 and 6 fold

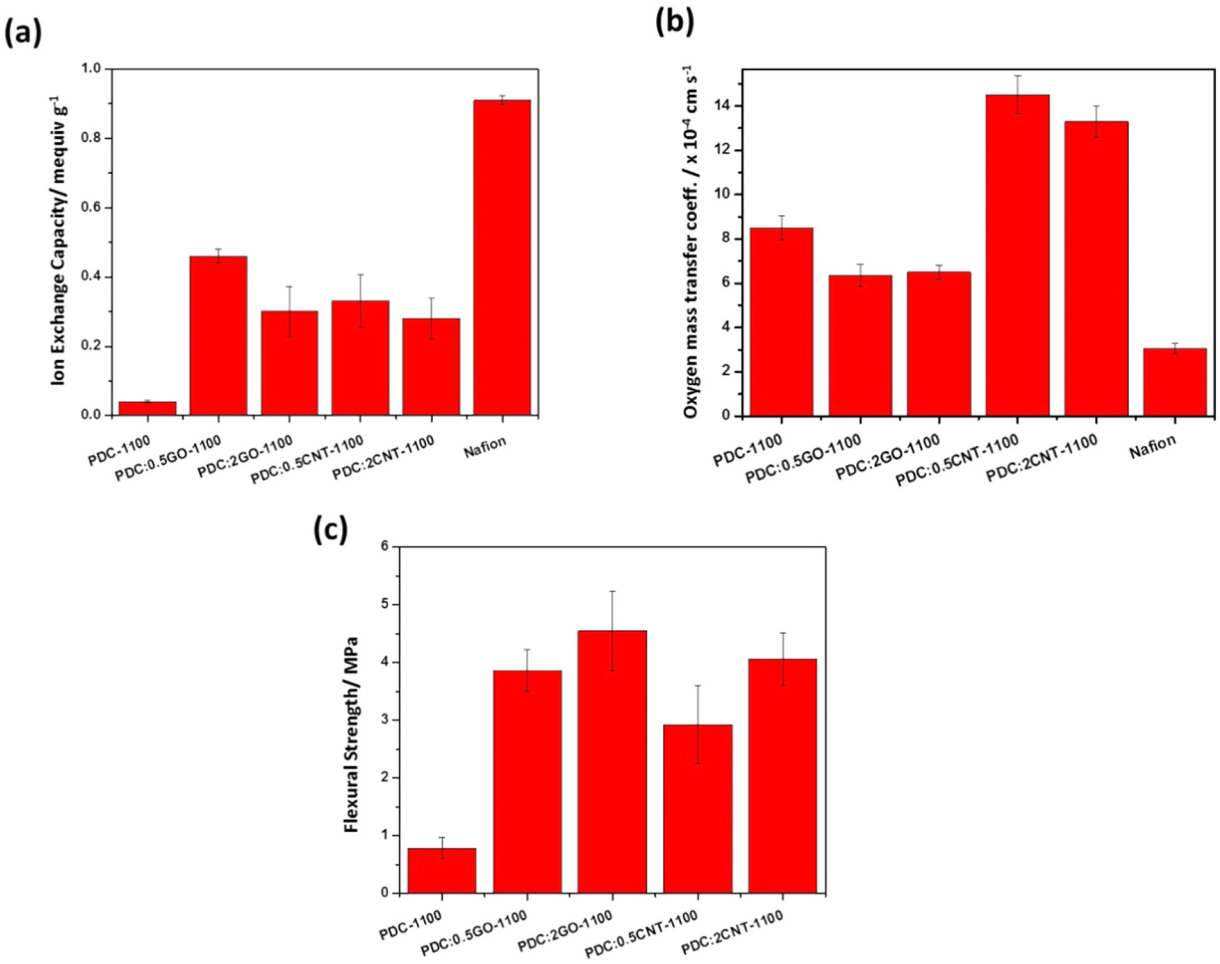

Fig. 6. (a) Ion exchange capacity measured for as prepared membranes compared with Nafion, (b) Oxygen mass transfer coefficient of PDC membranes, and (c) Flexural strength of the PDC membranes.

higher than the IECs of PDC-1100, owing to the proton-conducting nature of the well dispersed GO network in the PDC matrix [25]. The decrease in IEC value of PDC:2GO-1100 membrane due to the existence of reduced GO in the matrix, which led to less hydrophilic property. Similarly, for the PDC:0.5CNT-1100 and PDC:2CNT-1100 specimens, the corresponding IEC magnitudes increased drastically to 0.33 and 0.28 meq g^{-1}, respectively. Lee et al. found that the addition of GO in Nafion membrane results in increased ion conducting property and similarly Zhu et al. found that the presence of tubular channels in the MWCNT enhanced their ionic conduction properties [46,47]. Moreover, high loading of graphitic filler material to PDC material leads to high electrical conductivity, which resulted in decrease in ionic conductivity [39]. The observed IEC value of PDC:0.5GO-1100 and PDC:0.5CNT-1100 was almost half and one third of IEC value of polymeric Nafion, respectively.

4.5. Oxygen permeability

The oxygen permeability of the membrane is an important factor that directly affects the efficiency of MFC. The diffusion of oxygen through the membrane from the cathodic chamber to the anodic chamber leads to the creation of a mixed potential in the anodic chamber and disturbs its anaerobic condition because oxygen molecules act as an electron acceptor and inhibit the reaction at the anode for thermodynamic reasons [48]. The measured oxygen mass transfer coefficients of the membranes are shown in Fig. 6b. Since the oxygen mass transfer and diffusion coefficients of the materials for application in MFCs should be as small as possible, the PDC:0.5GO-1100 composite membrane demonstrated the best performance with the corresponding values equal to 6.37×10^{-4} cm s^{-1} and 1.91×10^{-4} cm^2 s^{-1}, respectively. This phenomenon is mainly because of high hydrophilic nature and small pore size results in low oxygen diffusion. Even though, PDC:0.5GO-1100 and PDC:2GO-1100 membranes have almost similar pore size but the hydrophilic property of PDC:0.5GO-1100 membrane is much higher than PDC:2GO-1100 membrane. For instance, Atwater et al. reported that the hydrophilic properties of the membrane inhibited the permeation of DO molecules through the membrane due to their non-polar characteristics [49]. On the other hand, the samples containing 0.5 and 2 wt% of CNTs pyrolyzed at 1100 °C exhibited higher oxygen mass transfer and diffusion coefficients as compared to those of the PDC-1100 samples. Usually, the incorporation of MWCNTs decreases these parameters, since the introduction of nanocomposites tends to block the diffusion paths for oxygen permeation. However, the PDC:0.5CNT-1100 and PDC:2CNT-1100 membranes possessed the large pore sizes of 735 nm and 619 nm, respectively, which resulted in high oxygen mass transfer and diffusion coefficients. This factor tremendously affects the final power production of MFCs.

4.6. Mechanical properties

The flexural strength of a membrane is one of the most important properties of the separator used in MFC. In this study, ring-on-ring ball bending test was performed to evaluate the effects of the pyrolysis temperature and addition of GO and MWCNTs on the flexural strengths of the PDC composite membranes (Fig. 6c). The flexural load-displacement curves indicate nearly elastic deformation followed by a

stage, during which the flexural strength increases until rupture. It is also evident that the flexural strength increases with the addition of graphitic filler material to ceramic matrix, which can be attributed to strong interfacial bonding between the graphitic filler and the ceramic matrix [50].

The membrane containing 0.5 wt% GO in the SiOC matrix demonstrated a significant increase in the flexural strength from 0.782 to 3.862 MPa at a pyrolysis temperature of 1100 °C. This effect is very likely to be resulted from the cross-linking of the polysiloxane matrix with functional groups of GO above 200 °C, which reduced the curing temperature [51]. Further increase in the GO loading to 2 wt% produced very small flexural strength increments of only 17% compared to 0.5 wt% loaded PDC membrane. This phenomenon might be due to the saturation limit of filler in the PDC matrix. Similar to the GO filler, MWCNTs were composite with the polysiloxane matrix, which increased its mechanical strength as compared to that of the bare SiOC membrane. Thus, the flexural strengths of SiOC loaded with 0.5 wt% MWCNTs and pyrolyzed at 1100 °C was 2.926 MPa. After increasing the MWCNT content to 2 wt%, the flexural strength of the membrane was increased, which was similar to the effect observed after GO addition.

4.7. Power generation and polarization curves

The bare PDC membranes and membranes containing 0.5 wt% graphitic fillers prepared at 1100 °C were selected as the separator materials for MFC and performance difference was evaluated because of differences in physical properties of the separators, such as IEC, mechanical stability, oxygen permeability, and water-to-heptane adsorption ratio. The PDC:0.5GO-1100 membrane exhibited higher water-to-heptane adsorption ratios, IEC values, mechanical stability and low oxygen permeability as compared to that of the PDC-1100 samples. On the other hand, the oxygen permeability of the PDC:0.5CNT-1100 membrane was higher than the magnitudes obtained by the other membranes, which can significantly deteriorate the performance of MFC. However, the other physical properties of these two membranes were noticeably better than that of PDC-1100 membrane. Evaluating the performance of MFCs utilizing PDC-1100, PDC:0.5GO-1100, and PDC:0.5CNT-1100 membranes could thus provide the information on the most influential physical property for selecting a suitable membrane separator for application in MFC.

During the first 20 days of operation of MFC, an electroactive biofilm grew on the surface of anode, which ultimately caused voltage fluctuations due to the immature biofilm. After five feed cycles, the MFCs were able to generate stable OV and OCV values. The MFC containing PDC:0.5GO-1100 produced an OV of 245 ± 3 mV, which exceeded the values obtained for PDC-1100 and the polymeric Nafion membrane by 15% and 35%, respectively. On the other hand, the MFC with the PDC:0.5CNT-1100 membrane exhibited an average OV of 170 ± 5 mV, which was significantly lesser than that of the bare PDC-1100 membrane. This decrement was mainly influenced by the high oxygen permeability between the cathode and the anode caused by the larger pore sized membrane. Furthermore, the internal resistance of the MFCs was strongly affected by the overpotential losses at anode and cathode as well as by the ohmic resistance of the membrane–electrolyte interfaces. In this work, the MFC containing the PDC:0.5CNT-1100 membrane had an internal resistance of 141 Ω, which was clearly higher than those of the MFCs with the PDC-1100 (137 Ω) and PDC:0.5GO-1100 (123 Ω) membranes. The performance of MFC in terms of the power density resembled the trends observed for OV and OCV (Fig. 7). The power density of the MFC with the PDC:0.5GO-1100 membrane was found to be 7.23 W m^{-3}, which was nearly 1.15 times higher than the MFC containing PDC-1100 membrane. Moreover, the power density obtained in MFC using PDC:0.5GO-1100 membrane was slightly higher than the power density produced by the MFC using Nafion membrane. The anode and cathode polarization

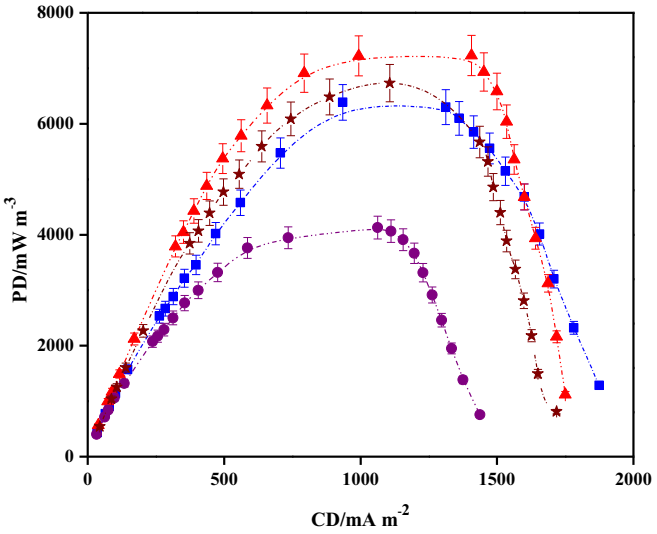

Fig. 7. Power density *vs.* current density curves obtained for MFCs with PDC-1100, PDC:0.5GO-1100, PDC:0.5CNT-1100, and compared with commercial Nafion membrane (PDC-1100; PDC:0.5GO-1100; PDC:0.5CNT-1100; Nafion).

curves suggested that there is hardly any variation in anode and cathode potential trends for all the MFCs, which further emphasize the change in the performance of MFC was mainly due to membrane properties not because of other influences (Fig. 8).

Although the polymeric Nafion membrane exhibited higher ion exchange capacity and lower oxygen permeability, the performance of MFC using this membrane was slightly inferior than the performance of MFC with PDC:0.5GO-1100 membrane giving best performance among all. The Nafion membrane transports protons due to the presence of a negatively charged sulfonic acid in the polymeric backbone. However, during the long-term operation of the MFC, containing the Nafion membrane, it can cause deactivation of proton-exchange sulfonic acid groups present in Nafion, which might have affected the performance of MFC. Another plausible explanation is that the transport of other cations through Nafion membrane (K^+, Na^+, Mg^+, Ca^+) through electrodialysis process, rather than proton driven by the concentration gradient, may reduce down its efficacy [52]. In an investigation, it was

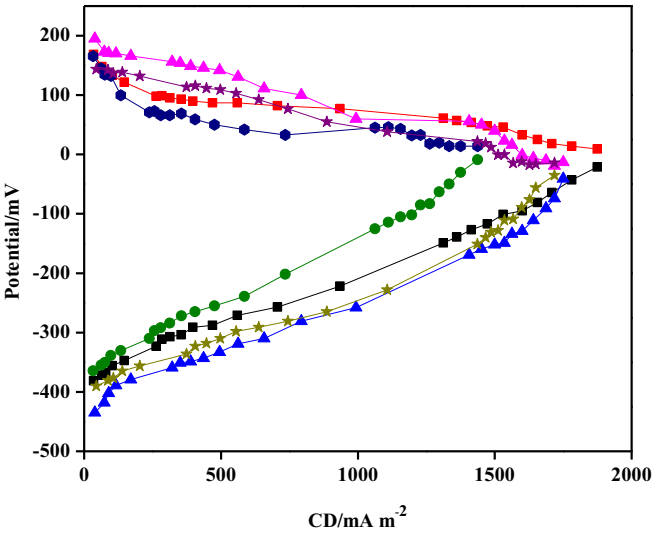

Fig. 8. Anode potential and cathode potential curves of MFCs with PDC-1100, PDC:0.5GO-100, PDC:0.5CNT-1100, and Nafion (AP(PDC-1100); CP(PDC-1100); AP(PDC:0.5GO-1100); CP(PDC:0.5GO-1100); AP(PDC:0.5CNT-1100); CP(PDC:0.5CNT-1100); AP(Nafion); CP(Nafion)).

found that the number of cations flowing through Nafion membrane from anodic to cathodic chamber was almost the same as the number of electrons transferred through the external circuit, which may drastically affect the performance of MFC [53]. Recently, Flimban et al. demonstrated that the biofouling of the polymeric Nafion membrane observed during the long-term operation of the MFC is another major factor affecting the performance of MFC [6].

On the other hand, possible proton-conduction mechanisms have not been extensively studied for porous ceramic membranes. However, it is likely that these mechanisms involve the osmotic and electro-osmotic drag forces. Many researchers claimed that the vehicle mechanism of the proton conductivity in porous ceramic membranes was the most probable one [54]. In this mechanism, the membrane adsorbs water molecules that are further protonated to form ionic clusters such as hydronium ions (H_3O^+), which penetrate through the medium *via* molecular diffusion causing proton transfer. These water molecules adsorb in the porous channels of the ceramic membrane further promoting the molecular diffusion of H_3O^+ ions from the anodic chamber to the cathodi chamber.

Water movement through the ceramic membrane of the MFC can proceed *via* two different routes. The first route corresponds to the active transport due to the electro-osmotic drag force in the closed circuit mode (under load), which is linearly related to the current generated by MFC. The second route is the passive transport induced by the osmotic pressure gradient between the dissimilar solutions in the anodic and cathodic chambers, which is dominant under open circuit conditions. The MFC utilizing macroporous PDC:0.5GO-1100 membrane generated relatively high power and current density at a low internal resistance because of its high water-to heptane ratio (hydrophilicity) as compared to those of all other PDC membranes prepared in this work. These hydrophilic characteristics, as well as the porous structure of the membrane, promote the adsorption of water molecules in its pores. Furthermore, enhanced ion conduction in the membrane is demonstrated by its high IEC value. These physical properties of the membrane (such as its hydrophilic characteristics, porous structure, and IEC) facilitate the proton transfer from the anodic to the cathodic chamber.

Although PDC-1100 membrane exhibited similar porous structure, its hydrophilic characteristics are lesser than the PDC:0.5GO-1100 membrane, which inhibit the adsorption of water molecules and limit the diffusion of hydronium ions. On the other hand, the PDC:0.5CNT-1100 membrane has higher water-to-heptane ratio and IEC as compared to those of the PDC-1100 membrane. However, the performance of MFC using PDC:0.5CNT-1100 membrane was considerably weaker than that of the PDC-1100 membrane due to the high permeability of oxygen from the cathodic to the anaerobic anodic chamber. This phenomenon reduced the performance of MFC, because of the voltage loss caused by the increase in redox potential due to either substrate consumption or the loss by aerobic oxidation rather than anaerobic fermentation. Moreover, since oxygen is a strong electron acceptor, it competes with the anode during the electron accepting process, negatively affecting the performance of MFC. Overall, the high power output observed from MFC using PDC:0.5GO-1100 shows that, the properties like hydrophilic characteristics and oxygen permeability could be the influential parameter for membrane performance in MFC.

4.8. Wastewater treatment and coulombic efficiency

The wastewater treatment efficiency in terms of COD removal was monitored for 10 batch cycles with the retention time of 3 days. After the stable phase of operation, all MFCs demonstrated COD removal efficiencies in the range of 87–91% (Fig. 9a). The average COD removal efficiencies of the MFCs containing the PDC-1100, PDC:0.5GO-1100, and PDC:0.5CNT-1100 membranes were 89 ± 1%, 87 ± 1%, and 83 ± 1%, respectively. The high COD removal efficiency suggests slight improvement in the kinetics of anodic oxidation caused by the rapid scavenging of protons through the porous ceramic membrane [55]. Moreover, the stacking of protons in the anodic chamber increases the acidity value, which decreases the microbial catalysis kinetic activity in the anodic chamber. The COD removal efficiency of the MFC with the Nafion membrane was equal to 91 ± 2%, which was comparable with the MFC containing the PDC ceramic membranes prepared at 1100 °C.

The MFC operated with the PDC:0.5GO-1100 membrane demonstrated CE of 28.8 ± 0.7%, which was 1.2 time higher than that of MFCs containing the PDC-1100 membrane (Fig. 9b). The CE value of the MFC with the Nafion membrane was 20.5 ± 0.6%, which was 29% lower than that of the MFC containing the PDC:0.5GO-1100 membrane. The NER studies also followed almost the same trend with PDC:0.5GO-1100 being the highest followed by Nafion > PDC-1100 > PDC:0.5CNT-1100 (Table 2). Thus, the performance evaluation demonstrated that PDC:0.5GO-1100 membrane exhibits superior proton conducting properties and can be a potential candidate to be used as an alternative to the extensively used Nafion 117 membrane for large scale applications of MFC.

5. Conclusions

Graphitic carbon modified PDC composite membranes were synthesized using a polysiloxane precursor and graphitic carbon fillers such as GO and MWCNTs. The PDC-based samples prepared in this study exhibited a porous structure with an open porosity ranging from 31% to 43%. The mechanical stability and IEC of the PDC matrix were considerably

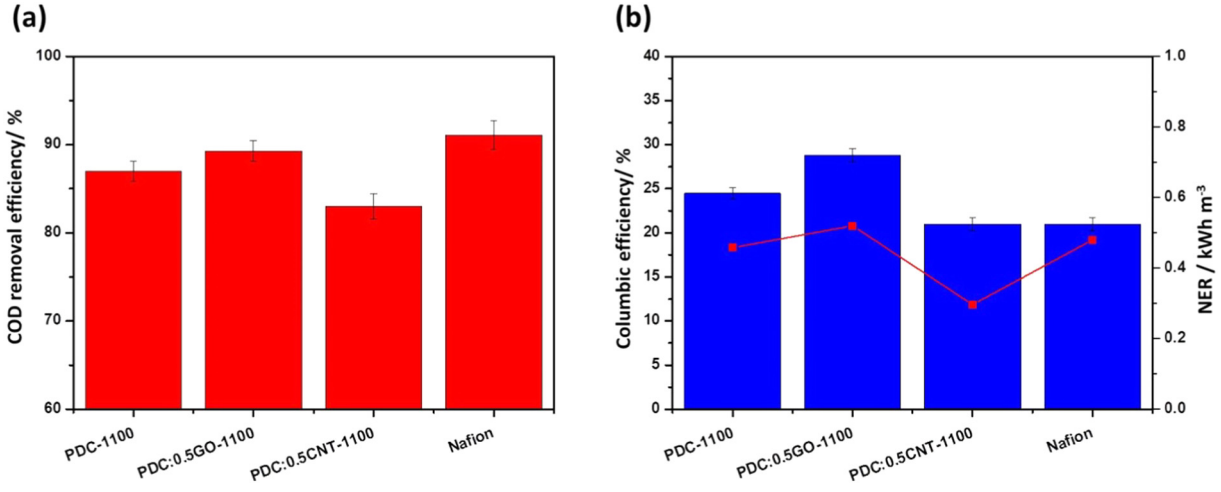

Fig. 9. (a) Average COD removal efficiency of MFC; (b) Average columbic efficiency and Normalized energy recovery of MFC using ceramic membranes and polymeric Nafion membrane.

Table 2
Electrochemical analysis data for all the MFCs.

Parameters	PDC-1100	PDC:0.5GO-1100	PDC:0.5CNT-1100	Nafion	Mullite [14]	Alumina [14]	Earthenware [14]
OV (mV)	213.60 ± 2.67	245.00 ± 3.46	170.20 ± 4.56	181.80 ± 3.51	–	–	–
OCV(mV)	621.70 ± 4.32	636.80 ± 3.19	546.90 ± 4.20	586.70 ± 2.66	519.8 ± 13.1	474.6 ± 7.7	529.0 ± 2.4
MPD (mW m^{-3})	6300	7232	4128	6733	4980	2600	6850
Internal resistance (Ω)	137	123	141	160	500	2000	304
COD removal efficiency (%)	87.00 ± 1.15	89.30 ± 1.15	83.00 ± 1.41	90.80 ± 1.86	41.5 ± 5.9	49.4 ± 7.3	50.2 ± 3.7
CE (%)	24.47 ± 0.31	28.81 ± 0.73	20.98 ± 0.77	20.48 ± 0.64	–	–	–
NER (kWh m^{-3})	0.45	0.52	0.29	0.48	–	–	–

improved by the incorporation of GO and MWCNT species. The samples containing 0.5 wt% of GO and MWCNTs featured a high mechanical stability, corresponding to 5-fold and 4-fold increase in the flexural strength of the bare PDC membrane pyrolyzed at 1100 °C. The PDC:0.5GO-1100 membrane possessed the highest water-to-heptane ratio and an IEC value of 0.46 meq g^{-1}, which was equal to 50% of the magnitude obtained for the Nafion membrane. Moreover, the oxygen diffusion coefficient was decreased from 4.03×10^{-4} cm^2 s^{-1} for the PDC-1100 membrane to 1.91×10^{-4} cm^2 s^{-1} for the PDC:0.5GO-1100 membrane. Owing to the superior hydrophilic characteristics and minimal oxygen permeability of the PDC:0.5GO-1100 membrane, the corresponding MFC exhibited coulombic efficiency values that was much higher than those of the MFC with the polymeric Nafion membrane. Therefore, the as-prepared PDC composite ceramic membranes can be potentially utilized as the membrane materials for large scale MFC applications.

Declaration of Competing Interest

The authors declare no competing financial interest.

Acknowledgement

We thank the German Federal Ministry of Education and Research (BMBF), INNO INDIGO Partnership Program (01DQ15013) and German Research Foundation (DFG), Research Training Group GRK 1860 "Micro-, meso- and macroporous nonmetallic Materials: Fundamentals and Applications" (MIMENIMA) and Department of Biotechnology, Government of India (BT/IN/INNO-INDIGO/28/MMG/2015-16) for providing financial support to complete this research work.

Appendix A. Supplementary data

Supplementary data to this article can be found online at https://doi.org/10.1016/j.bioelechem.2019.06.002.

References

[1] R. Kumar, L. Singh, A. Zularisam, F.I. Hai, Microbial fuel cell is emerging as a versatile technology: a review on its possible applications, challenges and strategies to improve the performances, Int. J. Energy Res. 42 (2018) 369–394.
[2] Y. Asensio, C. Fernandez-Marchante, J. Lobato, P. Cañizares, M. Rodrigo, Influence of the ion-exchange membrane on the performance of double-compartment microbial fuel cells, J. Electroanal. Chem. 808 (2018) 427–432.
[3] W. Liu, H. Jia, J. Wang, H. Zhang, C. Xin, Y. Zhang, Microbial fuel cell and membrane bioreactor coupling system: recent trends, Environ. Sci. Pollut. Res. (2018) 1–14.
[4] H.A. Patel, N. Mansor, S. Gadipelli, D.J. Brett, Z. Guo, Superacidity in Nafion/MOF hybrid membranes retains water at low humidity to enhance proton conduction for fuel cells, ACS Appl. Mater. Interfaces 8 (2016) 30687–30691.
[5] S. Das, K. Dutta, D. Rana, Polymer electrolyte membranes for microbial fuel cells: a review, Polym. Rev. (2018) 1–20.
[6] S.G. Flimban, S.H. Hassan, M.M. Rahman, S.-E. Oh, The effect of Nafion membrane fouling on the power generation of a microbial fuel cell, Int. J. Hydrog. Energy (2018) [in press].
[7] M. Do, H. Ngo, W. Guo, Y. Liu, S. Chang, D. Nguyen, L. Nghiem, B. Ni, Challenges in the application of microbial fuel cells to wastewater treatment and energy production: a mini review, Sci. Total Environ. 639 (2018) 910–920.
[8] F. Zhu, W. Wang, X. Zhang, G. Tao, Electricity generation in a membrane-less microbial fuel cell with down-flow feeding onto the cathode, Bioresour. Technol. 102 (2011) 7324–7328.
[9] J.R. Kim, G.C. Premier, F.R. Hawkes, R.M. Dinsdale, A.J. Guwy, Development of a tubular microbial fuel cell (MFC) employing a membrane electrode assembly cathode, J. Power Sources 187 (2009) 393–399.
[10] P.V. Moharir, A. Tembhurkar, Comparative performance evaluation of novel polystyrene membrane with ultrex as proton exchange membranes in microbial fuel cell for bioelectricity production from food waste, Bioresour. Technol. 266 (2018) 291–296.
[11] S. Ayyaru, P. Letchoumanane, S. Dharmalingam, A.R. Stanislaus, Performance of sulfonated polystyrene–ethylene–butylene–polystyrene membrane in microbial fuel cell for bioelectricity production, J. Power Sources 217 (2012) 204–208.
[12] S.S. Lim, W.R.W. Daud, J.M. Jahim, M. Ghasemi, P.S. Chong, M. Ismail, Sulfonated poly (ether ether ketone)/poly (ether sulfone) composite membranes as an alternative proton exchange membrane in microbial fuel cells, Int. J. Hydrog. Energy 37 (2012) 11409–11424.
[13] P.N. Venkatesan, S. Dharmalingam, Characterization and performance study of phase inversed sulfonated poly ether ether ketone–silico tungstic composite membrane as an electrolyte for microbial fuel cell applications, Renew. Energy. 102 ((2017) 77–86.
[14] G. Pasternak, J. Greenman, I. Ieropoulos, Comprehensive study on ceramic membranes for low-cost microbial fuel cells, ChemSusChem 9 (2016) 88–96.
[15] A.N. Ghadge, M. Ghangrekar, Development of low cost ceramic separator using mineral cation exchanger to enhance performance of microbial fuel cells, Electrochim. Acta 166 (2015) 320–328.
[16] A. Lale, M. Schmidt, M.D. Mallmann, A.V.A. Bezerra, E.D. Acosta, R.A.F. Machado, U.B. Demirci, S. Bernard, Polymer-derived ceramics with engineered mesoporosity: from design to application in catalysis, Surf. Coat. Technol. 350 (2018) 569–586.
[17] W. Fortuniak, P. Pospiech, U. Mizerska, J. Chojnowski, S. Slomkowski, A. Nyczyk-Malinowska, A. Wojteczko, E. Wisla-Walsh, M. Hasik, Generation of meso-and microporous structures by pyrolysis of polysiloxane microspheres and by HF etching of SiOC microspheres, Ceram. Int. 44 (2018) 374–383.
[18] P. Du, X. Wang, I.-K. Lin, X. Zhang, Effects of composition and thermal annealing on the mechanical properties of silicon oxycarbide films, Sens. Actuators A 176 (2012) 90–98.
[19] L. Duan, Q. Ma, Effect of pyrolysis temperature on the pore structure evolution of polysiloxane-derived ceramics, Ceram. Int. 38 (2012) 2667–2671.
[20] Z. Wu, X. Cheng, L. Zhang, J. Li, C. Yang, Sol-gel synthesis of preceramic polyphenylsilsesquioxane aerogels and their application toward monolithic porous SiOC ceramics, Ceram. Int. 44 (2018) 14947–14951.
[21] V. Ahilan, M. Wilhelm, K. Rezwan, Porous polymer derived ceramic (PDC)-montmorillonite-$H_3PMo_{12}O_{40}/SiO_2$ composite membranes for microbial fuel cell (MFC) application, Ceram. Int. 44 (2018) 19191–19199.
[22] C. Shen, E. Barrios, L. Zhai, Bulk polymer-derived ceramic composites of graphene oxide, ACS Omega 3 (2018) 4006–4016.
[23] R. Bhandavat, G. Singh, Synthesis, characterization, and high temperature stability of Si (B) CN-coated carbon nanotubes using a boron-modified poly (ureamethylvinyl) Silazane chemistry, J. Am. Ceram. Soc. 95 (2012) 1536–1543.
[24] J. Wang, C. Gong, S. Wen, H. Liu, C. Qin, C. Xiong, L. Dong, Proton exchange membrane based on chitosan and solvent-free carbon nanotube fluids for fuel cells applications, Carbohydr. Polym. 186 (2018) 200–207.
[25] M.R. Karim, K. Hatakeyama, T. Matsui, H. Takehira, T. Taniguchi, M. Koinuma, Y. Matsumoto, T. Akutagawa, T. Nakamura, S.-i. Noro, Graphene oxide nanosheet with high proton conductivity, J. Am. Chem. Soc. 135 (2013) 8097–8100.
[26] S. Khilari, S. Pandit, M.M. Ghangrekar, D. Pradhan, D. Das, Graphene oxide-impregnated PVA–STA composite polymer electrolyte membrane separator for power generation in a single-chambered microbial fuel cell, Ind. Eng. Chem. Res. 52 (2013) 11597–11606.
[27] Y.-L. Liu, Y.-H. Su, C.-M. Chang, D.-M. Wang, J.-Y. Lai, Preparation and applications of Nafion-functionalized multiwalled carbon nanotubes for proton exchange membrane fuel cells, J. Mater. Chem. 20 (2010) 4409–4416.
[28] F.I. Müller, C.A. Ferreira, D.S. Azambuja, C. Alemán, E. Armelin, Measuring the proton conductivity of ion-exchange membranes using electrochemical impedance spectroscopy and through-plane cell, J. Phys. Chem. B 118 (2014) 1102–1112.
[29] S. Kondaveeti, J. Lee, R. Kakarla, H.S. Kim, B. Min, Low-cost separators for enhanced power production and field application of microbial fuel cells (MFCs), Electrochim. Acta 132 (2014) 434–440.
[30] G. Jadhav, M. Ghangrekar, Performance of microbial fuel cell subjected to variation in pH, temperature, external load and substrate concentration, Bioresour. Technol. 100 (2009) 717–723.
[31] W.E. Federation, A.P.H. Association, Standard Methods for the Examination of Water and Wastewater, American Public Health Association (APHA), Washington, DC, USA, 2005.

[32] H.-J. Kleebe, Y.D. Blum, SiOC ceramic with high excess free carbon, J. Eur. Ceram. Soc. 28 (2008) 1037–1042.
[33] A.D. Dobrzańska-Danikiewicz, W. Wolany, D. Łukowiec, K. Jurkiewicz, P. Niedziałkowski, Characteristics of multiwalled carbon nanotubes-rhenium nanocomposites with varied rhenium mass fractions, Nanomater. Nanotechnol. 7 (2017), 1847980417707173.
[34] J. Zhang, H. Yang, G. Shen, P. Cheng, J. Zhang, S. Guo, Reduction of graphene oxide via L-ascorbic acid, Chem. Commun. 46 (2010) 1112–1114.
[35] A.A. King, B.R. Davies, N. Noorbehesht, P. Newman, T.L. Church, A.T. Harris, J.M. Razal, A.I. Minett, A new Raman metric for the characterisation of graphene oxide and its derivatives, Sci. Rep. 6 (2016), 19491.
[36] S. Fang, D. Huang, R. Lv, Y. Bai, Z.-H. Huang, J. Gu, F. Kang, Three-dimensional reduced graphene oxide powder for efficient microwave absorption in the S-band (2–4 GHz), RSC Adv. 7 (2017) 25773–25779.
[37] Y. Lou, G. Liu, S. Liu, J. Shen, W. Jin, A facile way to prepare ceramic-supported graphene oxide composite membrane via silane-graft modification, Appl. Surf. Sci. 307 (2014) 631–637.
[38] V. Yousefi, D. Mohebbi-Kalhori, A. Samimi, Application of layer-by-layer assembled chitosan/montmorillonite nanocomposite as oxygen barrier film over the ceramic separator of the microbial fuel cell, Electrochim. Acta 283 (2018) 234–247.
[39] P. Moni, M. Wilhelm, K. Rezwan, The influence of carbon nanotubes and graphene oxide sheets on the morphology, porosity, surface characteristics and thermal and electrical properties of polysiloxane derived ceramics, RSC Adv. 7 (2017) 37559–37567.
[40] D. Qian, E.C. Dickey, R. Andrews, T. Rantell, Load transfer and deformation mechanisms in carbon nanotube-polystyrene composites, Appl. Phys. Lett. Lexington (2000) 2868–2870.
[41] J.P. Salvetat, G.A.D. Briggs, J.-M. Bonard, R.R. Bacsa, A.J. Kulik, T. Stöckli, N.A. Burnham, L. Forró, Elastic and shear moduli of single-walled carbon nanotube ropes, Phys. Rev. Lett. (1999) 944–947.
[42] G.S.d. Reis, C.H. Sampaio, E. Lima, M. Wilhelm, Preparation of novel adsorbents based on combinations of polysiloxanes and sewage sludge to remove pharmaceuticals from aqueous solutions, Colloids Surf. A Colloids Surf. A. 2016 (2016) 304–315.
[43] B.B. Munavalli, M.Y. Kariduraganavar, Development of novel sulfonic acid functionalized zeolites incorporated composite proton exchange membranes for fuel cell application, Electrochim. Acta 296 (2019) 294–307.
[44] M. Naviroj, S. Miller, P. Colombo, K. Faber, Directionally aligned macroporous SiOC via freeze casting of preceramic polymers, J. Eur. Ceram. Soc. 35 (2015) 2225–2232.
[45] S. Stankovich, D.A. Dikin, R.D. Piner, K.A. Kohlhaas, A. Kleinhammes, Y. Jia, Y. Wu, S.T. Nguyen, R.S. Ruoff, Synthesis of graphene-based nanosheets via chemical reduction of exfoliated graphite oxide, carbon 45 (2007) 1558–1565.
[46] F. Zhu, K. Schulten, Water and proton conduction through carbon nanotubes as models for biological channels, Biophys. J. 85 (2003) 236–244.
[47] K.J. Lee, Y.H. Chu, Preparation of the graphene oxide (GO)/Nafion composite membrane for the vanadium redox flow battery (VRB) system, Vacuum 107 (2014) 269–276.
[48] A.S. Mathuriya, D. Pant, Assessment of expanded polystyrene as a separator in microbial fuel cell, Environ. Technol. (2018) 1–10.
[49] J.E. Atwater, J.R. Akse, Oxygen permeation through functionalized hydrophobic tubular ceramic membranes, J. Membr. Sci. 301 (2007) 76–84.
[50] L. An, W. Xu, S. Rajagopalan, C. Wang, H. Wang, Y. Fan, L. Zhang, D. Jiang, J. Kapat, L. Chow, Carbon-nanotube-reinforced polymer-derived ceramic composites, Adv. Mater. 16 (2004) 2036–2040.
[51] T.M. Robert, D. Augustine, D. Mathew, C.R. Nair, Graphene oxide induced fast curing of amino novolac phthalonitrile, RSC Adv. 5 (2015) 1198–1204.
[52] M. Rahimnejad, G. Bakeri, G. Najafpour, M. Ghasemi, S.-E. Oh, A review on the effect of proton exchange membranes in microbial fuel cells, Biofuel Res. J. 1 (2014) 7–15.
[53] R.A. Rozendal, H.V.M. Hamelers, C.J.N. Buisman, Effects of membrane cation transport on pH and microbial fuel cell performance, Environ. Sci. Technol. 40 (2006) 5206–5211.
[54] K.D. Kreuer, A. Rabenau, W. Weppner, Vehicle mechanism, a new model for the interpretation of the conductivity of fast proton conductors, Angew. Chem. 21 (1982) 208–209.
[55] B. Neethu, G. Bhowmick, M. Ghangrekar, Enhancement of bioelectricity generation and algal productivity in microbial carbon-capture cell using low cost coconut shell as membrane separator, Biochem. Eng. J. 133 (2018) 205–213.